Human Health Risk Assessment of CO2 Leakage into Overlying Aquifers Using a Stochastic, Geochemical Reactive Transport Approach

ARTICLE *in* ENVIRONMENTAL SCIENCE & TECHNOLOGY · APRIL 2013

Impact Factor: 5.33 · DOI: 10.1021/es400316c · Source: PubMed

3 AUTHORS:

Adam L. Atchley
Los Alamos National Laboratory
9 PUBLICATIONS **35** CITATIONS
SEE PROFILE

Reed Maxwell
Colorado School of Mines
185 PUBLICATIONS **2,705** CITATIONS
SEE PROFILE

Alexis Navarre-Sitchler
Colorado School of Mines
42 PUBLICATIONS **550** CITATIONS
SEE PROFILE

Journal of Contaminant Hydrology 165 (2014) 53–64

Contents lists available at ScienceDirect

Journal of Contaminant Hydrology

journal homepage: www.elsevier.com/locate/jconhyd

The effects of physical and geochemical heterogeneities on hydro-geochemical transport and effective reaction rates

Adam L. Atchley *, Alexis K. Navarre-Sitchler, Reed M. Maxwell

Department of Geology & Geological Engineering, USA
Hydrological Science & Engineering, USA

ARTICLE INFO

Article history:
Received 17 January 2014
Received in revised form 15 July 2014
Accepted 21 July 2014
Available online 28 July 2014

Keywords:
Hydro-geochemical transport
Physical and geochemical heterogeneities
Effective reaction rate

ABSTRACT

The role of coupled physical and geochemical heterogeneities in hydro-geochemical transport is investigated by simulating three-dimensional transport in a heterogeneous system with kinetic mineral reactions. Ensembles of 100 physically heterogeneous realizations were simulated for three geochemical conditions: 1) spatially homogeneous reactive mineral surface area, 2) reactive surface area positively correlated to hydraulic heterogeneity, and 3) reactive surface area negatively correlated to hydraulic heterogeneity. Groundwater chemistry and the corresponding effective reaction rates were calculated at three transverse planes to quantify differences in plume evolution due to heterogeneity in mineral reaction rates and solute residence time (τ). The model is based on a hypothetical CO_2 intrusion into groundwater from a carbon capture utilization and storage (CCUS) operation where CO_2 dissolution and formation of carbonic acid created geochemical dis-equilibrium between fluids and the mineral galena that resulted in increased aqueous lead (Pb^{2+}) concentrations. Calcite dissolution buffered the pH change and created conditions of galena oversaturation, which then reduced lead concentrations along the flow path. Near the leak kinetic geochemical reactions control the release of solutes into the fluid, but further along the flow path mineral solubility controls solute concentrations. Simulation results demonstrate the impact of heterogeneous distribution of geochemical reactive surface area in coordination with physical heterogeneity on the effective reaction rate ($K_{rxn,eff}$) and Pb^{2+} concentrations within the plume. Dissimilarities between ensemble Pb^{2+} concentration and $K_{rxn,eff}$ are attributed to how geochemical heterogeneity affects the time (τ_{eq}) and therefore advection distance (L_{eq}) required for the system to re-establish geochemical equilibrium. Only after geochemical equilibrium is re-established, $K_{rxn,eff}$ and Pb^{2+} concentrations are the same for all three geochemical conditions. Correlation between reactive surface area and hydraulic conductivity, either positive or negative, results in variation in τ_{eq} and L_{eq}.

Published by Elsevier B.V.

1. Introduction

Simulating reactive transport of aqueous solutes that chemically interact with aquifer mineralogy is essential to understand a wide range of Earth processes including chemical weathering (e.g. Maher, 2010; Moore et al., 2012; Navarre-Sitchler et al., 2011; Steefel et al., 2005), carbon capture utilization and storage (CCUS) (e.g. Apps et al., 2010; Navarre-Sitchler et al., 2013; Zheng et al., 2009), water quality (Atchley et al., 2013a; Carroll et al., 2009), and risk assessment (Atchley et al., 2013b; Siirila and Maxwell, 2012; Siirila et al., 2012). Of recent interest is CCUS impacts to groundwater where both hydrological and geochemical processes play an important role in understanding the potential for water quality degradation in the event of a CO_2 leak (Atchley et al., 2013a; Wilkin and Digiulio, 2010; Zheng et al., 2009). Recent work has suggested that increases in aqueous lead

* Corresponding author at: Earth and Environmental Sciences Division, Los Alamos National Laboratory, Los Alamos, NM, USA.
E-mail address: aatchley@lanl.gov (A.L. Atchley).

http://dx.doi.org/10.1016/j.jconhyd.2014.07.008
0169-7722/Published by Elsevier B.V.

(Pb^{2+}) concentrations from galena dissolution in reducing aquifers may occur due to a CO_2 intrusion into groundwater (Wang and Jaffe, 2004; Apps et al., 2010). The ultimate impact of Pb^{2+} concentrations on groundwater quality and human health is a product of plume spreading and time dependent geochemical reactions (Atchley et al., 2013b; Siirila et al., 2012). However, few published articles exist concerning the tightly coupled hydrological and geochemical processes of mineral dissolution and reactivation of mineral precipitation that shape transport and time dependent speciation of chemically reactive solutes. The goal of this work is to demonstrate the combined effects of physical and geochemical heterogeneities on mineral reaction rates in time and reactive solute transport length as an aquifer responds to geochemical disequilibrium induced by a hypothetical CO_2 leakage scenario.

Physical subsurface heterogeneity has been shown to govern mixing and spreading of conservative solutes (e.g. Cirpka and Kitanidis, 2000; Dagan, 1984; Mercado, 1967; Rubin, 1991; Sudicky, 1986; Yeh, 1992), but reactive solutes demonstrate added complexity as the chemical composition evolves when coupled with transport. For example, Atchley et al. (2013a) demonstrated that solute residence time governs solute conditions in a homogeneous geochemical system resulting in varied plume lengths due to reactions in fast or slow transport paths. Additionally, reaction rates resulting from kinetic disequilibrium between advected solute and the host material decrease with time and transported distance (Dentz et al., 2011; Lichtner, 1988; Navarre-Sitchler and Brantley, 2007; Scheibe et al., 2007; White and Brantley, 2003), causing non-linear changes to subsurface chemistry during groundwater transport. Often these rates of geochemical reactions are low (Bearup et al., 2012), and non-equilibrium conditions may exist throughout a plume. Therefore, the process of reaching equilibrium in hydrogeochemical transport can also shape solute characteristics at large scales even in geochemically homogeneous systems (Maher, 2010, 2011).

Like hydrologic heterogeneity, it is well known that aquifer mineralogy is also spatially heterogeneous and therefore will cause spatially variable geochemical reactive transport conditions (Barber et al., 1992; Tompson et al., 1996; van der Zee and van Remsdijk, 1991). In instances of heterogeneous geochemical conditions hydraulic heterogeneity can move reactive solutes to or away from areas of reactivity in transport limited conditions (Navarre-Sitchler et al., 2009, 2011; Li et al., 2010). Delineating the influence of heterogeneous hydrological processes versus geochemical processes has typically been a difficult task due to the dynamic interplay between reactions and transport. Here we simplify the problem and use spatially variable reactive mineral surface area correlated to hydraulic conductivity to elucidate contributions from physical and geochemical heterogeneities on reactive plume evolution.

Reactive mineral surface area is often negatively correlated to hydraulic conductivity because larger surface areas tend to accompany low hydraulic conductive areas (Barber et al., 1992; Seeboonruang and Ginn, 2006; Tompson et al., 1996; van der Zee and van Remsdijk, 1991). However, some studies show evidence for positively correlating reactive surface area to hydraulic conductivity, where packing order, grain size distribution, or mineral composition may reduce reactive surface areas in low hydraulic conductive areas (Allen-King et al., 1998; Holdren and Speyer, 1987; Robin et al., 1991; Scheibe et al., 2007). First-order biodegradation studies have also implemented positively and negatively correlated biodegradation rates to hydraulic conductivity in two-dimensional domains (Cunningham and Fadel, 2007). Negatively correlated biodegradation rates exhibited extended plume fingering, while positively correlated biodegradation rates reduce plume fingering and solute heterogeneity.

Effective reaction rates are often used to upscale heterogeneous rates of geochemical processes at small sub-grid-scale (pore to sub-meter scale) to a homogenized larger-scale (meter to tens of meters) discrete grid cell or representative elementary volume (REV) (Li et al., 2006, 2007; Meile and Tuncay, 2006; Navarre-Sitchler et al., 2009). At the REV scale, effective reaction rates can capture plume development only if each mineral phase of a geochemically heterogeneous system has the same net average fluid contact time as a homogenized geochemical system (Glassley et al., 2002). However, spatially heterogeneous reaction rates can appear at scales larger than the REV and therefore shape large-scale chemistry (Cunningham and Fadel, 2007; Maxwell et al., 2003, 2007; Scheibe et al., 2007; Tompson et al., 1996; Valocchi, 1989). A simulation of linear kinetic reactive transport over large-scale, two-dimensional physically and chemically heterogeneous domains found that homogeneous representations of linear reaction rates would only be valid if the chemical heterogeneity is much smaller than that of physical heterogeneity (Seeboonruang and Ginn, 2006). Yet to be tested is the role that non-linear kinetic reactions, as calculated using transition state theory (Aagaard and Helgeson, 1982; Steefel and Lasaga, 1994), play in determining the relevance of geochemical heterogeneity in a three-dimensional aquifer. Thus, in order to better understand the chemical state of a reactive plume and the effective parameters at any point, we investigate three-dimensional plume evolution within the non-equilibrium stages of reactive transport.

2. Methods

Monte Carlo ensembles of 100 three-dimensional heterogeneous subsurface realizations are used to simulate reactive transport. Mineral dissolution and resulting reactivation of precipitation are tracked at a sequence of planes transverse to the mean flow direction. Three geochemical scenarios are examined: 1) a homogeneous geochemical condition, 2) a positive correlation of reactive surface area to grid cell hydraulic conductivity, and 3) a negative correlation of reactive surface area to grid cell hydraulic conductivity. All three geochemical conditions are simulated over the same 100 heterogeneous flow fields for a simulation duration of 6000 days or approximately 16.5 years. Geochemical reactions are simulated as non-linear kinetically driven mass transfer reactions calculated by transition state theory (Aagaard and Helgeson, 1982; Steefel and Lasaga, 1994). The domain average reactive surface area is the same for each of the three geochemical ensembles simulated and the homogeneous geochemical domain represents a domain averaged reactive surface area. The positively and negatively correlated surface area ensembles have spatially heterogeneous geochemical conditions. Effective reaction rates ($K_{rxn,eff}$) and Pb^{2+} concentrations are compared within and across geochemical ensembles at a sequence of three planes (200 m, 400 m, and 600 m down gradient from the CO_2 source location, Fig. 1) and the pumping well (900 m from the CO_2

source, Fig. 1). This approach allows us to evaluate Pb^{2+} concentrations as the plume is transported down gradient toward the pumping well and geochemical equilibrium is re-established.

Reactive transport resulting from CO_2 intrusion into an aquifer is simulated along each of the one-dimensional streamlines mapped in the aquifer (described below) using CrunchFlow, a fully kinetic multi-component reactive transport code (Steefel, 2001; Steefel and Yabusaki, 1996). CO_2 leakage, continuous for the duration of the simulation, causes a decrease in aquifer pH as CO_2 dissolves in the water and forms carbonic acid (H_2CO_3). This reduction in pH drives galena and calcite dissolution (Table 1). Galena dissolution releases Pb^{2+} to solution. These two geochemical reactions are coupled through the proton concentration (pH). The rapid consumption of H^+ through calcite dissolution changes the saturation state of the water with respect to galena, and therefore the galena dissolution rates. As the pH is buffered by calcite dissolution in the higher Pb^{2+} waters just downstream of the CO_2 leak, the water oversaturates with respect to galena and galena precipitates from solution. For a complete description of the geochemical conditions and aquifer mineralogy used see Atchley et al. (2013a). Mass transfer as simulated by transition state theory represents dissolution reaction rates as a negative value while precipitation rates are a positive value; at geochemical equilibrium reaction rates are near zero where dissolution and

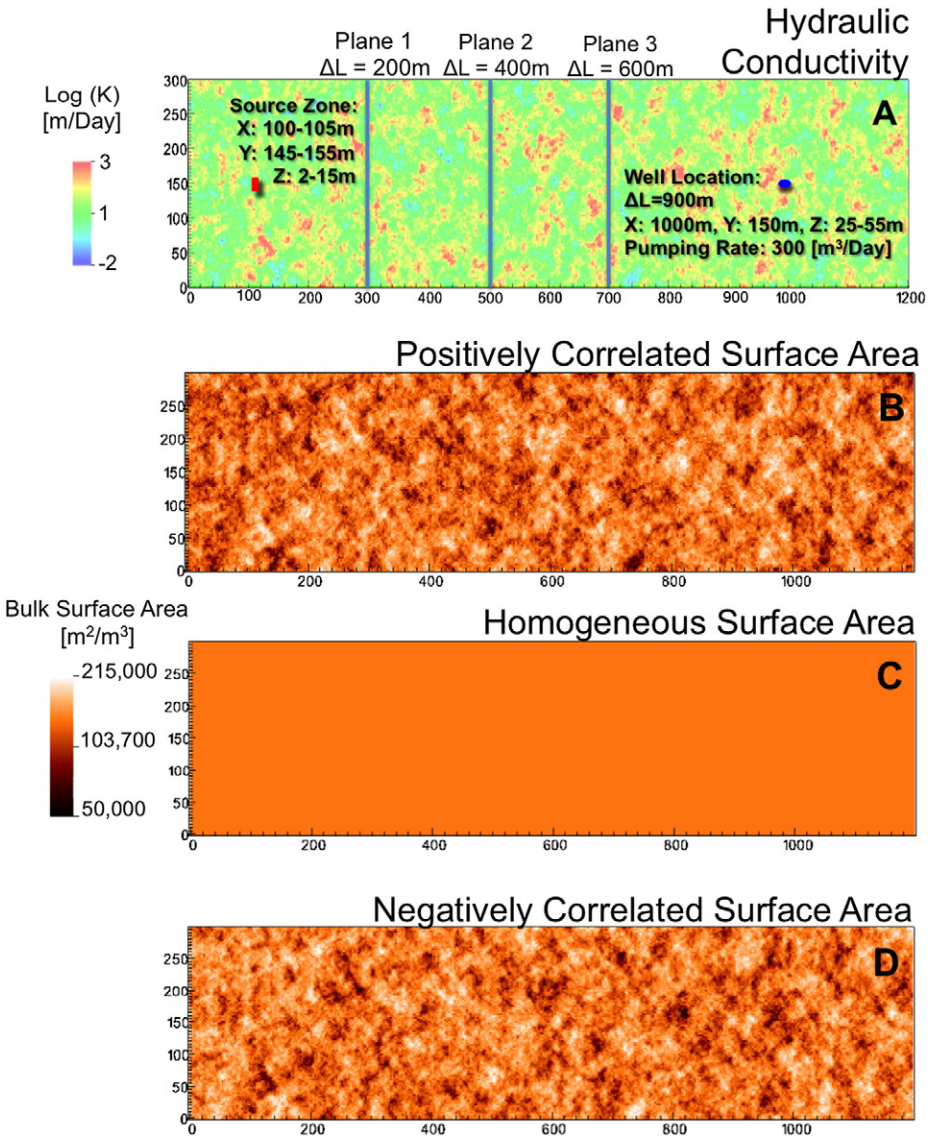

Fig. 1. Domain map of source zone, pumping well, and the three transverse planes. The longitudinal distance from the CO_2 source for each plane and pumping well is noted as ΔL in plot A overlaid on an example realization of a permeability field. Plot B shows a positively correlated surface area domain, plot C a homogeneous surface area domain, and plot D a negatively correlated surface area domain. The same permeability field example is used for all three geochemical representations. All views are planar.

Table 1
Ensemble average and range of A_m (bulk reactive surface area [m^2/m^3]).

Geochemical condition	Ave SA_{bulk}	Highest SA_{bulk}	Lowest SA_{bulk}	α	b
Calcite					
Negative	73,137	147,799	930	15,408.6	99,608
Positive	73,196	149,331	1074	15,408.6	46,725.8
Homogeneous	73,167				
Galena					
Negative	136,960	277,221	1307	28,947.2	186,688.3
Positive	137,070	280,100	1579	28,947.2	87,341.5
Homogeneous	137,015				

Mineral/aqueous species	Reaction stoichiometry	Rate constant k_m [$mol/m^2/s$] (log)	Log K_{sp} at 25 °C
Calcite	$CaCO_3 + H^+ \leftrightarrow Ca^{2+} + HCO_3^-$	−11.5	1.8487
CO_2 (aq)	$CO_2 + H_2O \leftrightarrow HCO_3^- + H^+$	–	10.329
Galena	$PbS + H^+ \leftrightarrow Pb^{2+} + HS^-$	−11	−14.8544
H_2S (aq)	$H_2S \leftrightarrow HS^- + H^+$	–	−7.9759

precipitation mass transfer are equal to each other. CrunchFlow accounts for changes in reactive surface area from mineral dissolution and precipitation reactions by

$$A_{m,dissolution} = A_{m,i}\left[\left(\frac{\phi}{\phi_i}\right)\left(\frac{\phi_m}{\phi_{m,i}}\right)^{2/3}\right]$$
$$A_{m,precipitation} = A_{m,i}\left[\left(\frac{\phi}{\phi_i}\right)\right]^{2/3} \quad (1)$$

where A_m is the bulk reactive surface area of mineral m and i is the initial condition. ϕ is the aquifer porosity, and $\phi_{m,i}$ is the volume fraction of mineral m at initial condition i. Therefore, kinetic reaction rates change in space due to changing plume conditions along the transport path, and change in time due to the changing reactive surface area of dissolving and precipitating minerals at a given point along the transport path. Changes in porosity from mineral dissolution and precipitation are assumed to be negligible, given that the bulk of the aquifer mineralogy is made up of non-reactive quartz (See Table 2 in Atchley et al., 2013a) and that small changes in porosity have a negligible effect to changes in flow (Obi and Blunt, 2006).

$K_{rxn,eff}$ [mol/m^2 day] values for galena dissolution were calculated for each ensemble of positively and negatively correlated surface areas, as well as the homogeneous ensemble by a dimensional analysis expressed as:

$$K_{rxn,eff}\left[\frac{mol}{m^2 day}\right] = \frac{\beta(C_0 - C)\phi}{\tau * A_{m,galena}} \times 1000\left[\frac{L}{m^3}\right]. \quad (2)$$

C_0 is the initial Pb^{2+} concentration [mol/L], which is 7.25×10^{-12} [mol/L]. C is the ensemble Pb^{2+} concentration measured at the planes or pumping well. β is the stoichiometric coefficient for Pb in galena, which is 1. $A_{m,galena}$ is the bulk surface area for galena [m^2/m^3] and ϕ is the porosity of the aquifer [m^3/m^3]. τ is the ensemble median residence time for each plane or the pumping well [days]. A conversion factor of 1000 [L/m^3] is used to convert from liters of groundwater to volume of groundwater.

The homogeneous geochemical condition has a bulk reactive surface area (SA_{bulk}) of 73,167 and 137,015 [m^2/m^3] for calcite and galena respectively (Table 1). The physical heterogeneity of the subsurface had a variance of hydraulic conductivity (σ^2_{lnK}) of 3.61. A heterogeneous correlation length of 10 [m] longitudinally and 1 [m] vertically was used with cell dimensions of $3 \times 3 \times 0.3$ [m]. Reactive surface areas were positively correlated to hydraulic conductivity (K_{hc}) and then negatively correlated to hydraulic conductivity (Fig. 1) by:

$$\text{Positive correlation} = SA_p = LOG(K_{hc}) * \alpha + b_p \quad (3)$$

$$\text{Negative correlation} = SA_n = LOG(K_{hc}) * (-\alpha) + b_n \quad (4)$$

where α and b describe the scale and relationship of the surface area correlation. α and b parameters were fitted such that both the positively and negatively correlated ensembles had the same domain average reactive surface area as the homogeneous reactive surface area ensemble. α was 15,408.6 and 28,947.2 for calcite and galena respectively. b_p was 46,725.8 and 87,341.5 for calcite and galena in the positively correlated

Table 2
τ_{eq} and corresponding simulation time for each ensemble. Ensemble median residence time, average $K_{rxn,eff}$, and average Pb^{2+}.

	Simulation time		Positive		Homogenous		Negative
τ_{eq} [day]	1000 [day]		481		481		492
	6000 [day]		482		482		495
	Median tau [day]	$K_{rxn,eff}$ [mol/m^2 day]	Pb [mol/L]	$K_{rxn,eff}$ [mol/m^2 day]	Pb [mol/L]	$K_{rxn,eff}$ [mol/m^2 day]	Pb [mol/L]
Plane 1 (ΔL = 200 m)	89.6	−4.53E−13	3.16E−11	−4.61E−13	3.2E−11	4.74E−13	3.27E−11
Plane 2 (ΔL = 400 m)	199.7	−1.52E−13	2.55E−11	−1.54E−13	2.57E−11	−1.58E−13	2.62E−11
Plane 3 (ΔL = 600 m)	377.8	−7.12E−14	2.34E−11	−7.12E−14	2.34E−11	−7.26E−14	2.37E−11
Well (ΔL = 900 m)	641.9	−3.93E−14	2.24E−11	−3.93E−14	2.24E−11	−3.96E−14	2.25E−11

case, and b_n was 99,608.0 and 186,688.3 for calcite and galena in the negatively correlated case. The ranges for reactive surface areas for the positively and negatively correlated cases are shown in Table 1. Relating the reactive surface area to the LOG(K_{hc}) equates to a smaller magnitude of chemical heterogeneity compared to physical heterogeneity. This relationship between reactive surface area and hydraulic conductivity tests the findings of Seeboonruang and Ginn (2006) that homogeneous representations of reaction rates are valid if chemical heterogeneity is much smaller than physical heterogeneity for non-linear kinetic reactions.

The streamline method described in Atchley et al. (2013a) is used to simulate kinetic geochemical reactive transport of CO_2 impacted groundwater from a CO_2 source area to a pumping well, located 900 m down gradient. The streamline methodology is a well-documented approach that reduces three-dimensional transport in space to a one-dimensional transport equation in time of flight or residence time (τ) (Crane and Blunt, 1999; Ginn, 2001; Ginn et al, 1995; Maxwell et al., 2003; Thiele et al., 1996). While mixing between streamlines is not considered in the streamline approach, macrodispersion and plume spreading are directly modeled and have been shown to accurately capture physical transport when the timescale for transverse dispersion is longer than the travel time through the system (Viswanathan and Valocchi, 2004). In this streamline application a collection of flux weighted streamlines is initiated at a pumping well and traced backwards through the domain for each realization. Streamline fluxes are assigned within each grid cell, noted as j, that the pumping well screen passes through by

$$Q_{STL} = \frac{Q_j}{l_{STL}} \tag{5}$$

where Q_j is the flux of water from grid cell j to the pumping well within grid cell j and l_{STL} is the number of streamlines seeded around the well in grid cell j. Q_j is found by

$$Q_j = Q_t\left(\frac{K_j}{K_{sum}}\right) \tag{6}$$

$$K_{sum} = \sum_{i=1}^{1\to n} K_i \tag{7}$$

where K_j is the hydraulic conductivity of grid cell j, and K_{sum} is the sum of all grid cell hydraulic conductivities that the entire pumping well screen passes through. Eqs. (5)–(7) dictate that each of the streamlines within a given realization has a unique flux that reflects the heterogeneous hydraulic conductivity of the aquifer. Collectively, these streamlines represent the water moving from a source to the pumping well through a three-dimensional aquifer. Given that each realization within the ensemble represents a unique, equally-probable physically heterogeneous domain, the spreading explicitly mapped by the streamlines results in unique flux of water between the CO_2 source zone and pumping well (Atchley et al., 2013a). Pb^{2+} concentrations calculated at the three planes are only from streamlines that are captured by the pumping well and cross the CO_2 source area, which results in a consistent volume of groundwater to analyze between the three planes and at the pumping well for each realization.

3. Results and discussion

3.1. Geochemistry along the streamlines

Residence time (τ) on a streamline at location reference ζ and the advected length (L) in the X direction over a corresponding distance (s) along the streamline are related as a function of the streamline tortuosity (ω) and velocity (v) of the fluid traveling through the porous media (Fig. 2) by the streamline transform

$$\tau = \int_0^s \frac{L(\zeta)}{v(\zeta)}\,d\zeta \tag{8}$$

where

$$L(\zeta) = X_{(\zeta)} - X_{(0)} = \frac{s}{\omega}. \tag{9}$$

The streamline transform allows a three-dimensional plume in space to be represented by individual 1D flow paths in time (Fig. 2). Thus, evolving Pb^{2+} concentrations along a single streamline plotted versus residence time (τ along the x-axis), depict geochemical conditions along a tortuous path through the aquifer. Each streamline has a unique relationship between τ and L, determined by variation in hydraulic conductivity along the streamline, which affects both fluid velocity and streamline tortuosity. The τ and L relationship of all streamlines along with local geochemical reactions in each grid cell determine the collective reaction progress at the transverse planes or pumping well.

Individual, deconvolved streamlines provide information about the geochemical reactions and rates within the aquifer. Pb^{2+} concentrations initially increase along the streamlines as galena dissolves within short residence times and then slowly decrease as galena precipitates (Fig. 2). These changes in Pb^{2+} concentration are the result of changes in the saturation state of galena. A drop in pH, resulting from CO_2 dissolution into the water, induces galena under saturation causing dissolution near the leak. Galena dissolution increases Pb^{2+} concentrations. The pH decrease also induces under saturation of fluid with respect to calcite, the dissolution of which buffers the pH change. Thus, calcite dissolution increases pH along the streamline and, in turn, causes the saturation state of galena to increase and ultimately galena becomes over saturated and precipitates. The precipitation of galena results in a gradual lowering of Pb^{2+} concentrations further along the streamline (Fig. 2). Eventually the fluid and minerals re-equilibrate and Pb^{2+} concentrations no longer change with increasing τ or L.

Reaction rates of galena and calcite change along the streamline as the fluid composition, and therefore degree of dis-equilibrium between the fluid and minerals, changes (Aagaard and Helgeson, 1982; Steefel and Lasaga, 1994). Local calcite reaction rates (computed in each grid cell) are the fastest near the source where the CO_2 leak induces geochemical dis-equilibrium and slow with increasing τ until the system re-equilibrates (Fig. 3). The τ of the advected fluid from the CO_2 source to the point of re-equilibrium where reaction rates approach zero is noted as τ_{eq}. The advection distance at which fluid equilibrates with aquifer material L_{eq} as defined by Maher (2010) is related to τ_{eq} by the streamline transform (Eq. (8)).

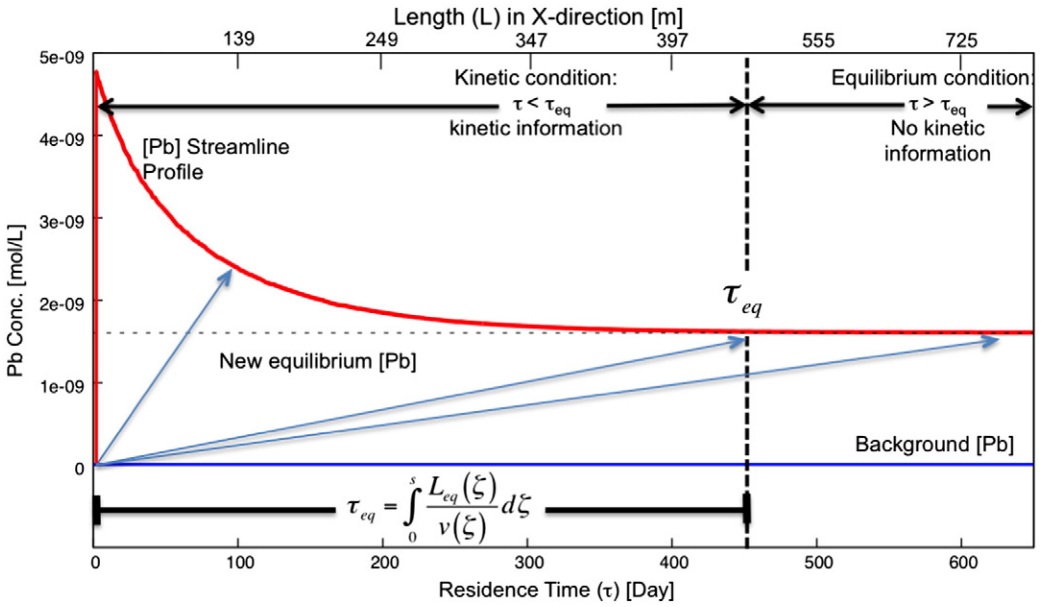

Fig. 2. A Pb^{2+} concentration profile of a representative streamline delineating τ_{eq}, background Pb concentrations, and the new Pb concentration at equilibrium. Negative values of the slope of the blue arrows represent effective galena dissolution reaction rates ($K_{rxn,eff}$). The relationship between residence time (τ) and advection length is shown with residence time plotted on the bottom x-axis and advection length in the x-direction of the flow domain plotted on top. Geochemical conditions that affect the reaction rate such as reactive surface area determine the residence time required to achieve τ_{eq}. The physical heterogeneity that determines speed of advection and reaction rate then defines the L_{eq}.

We term the zone where $\tau < \tau_{eq}$ the kinetic zone, in which non-linear kinetic reaction rates influence $K_{rxn,eff}$. The zone where $\tau > \tau_{eq}$ is noted as the equilibrium zone in which only residence time influences the observed $K_{rxn,eff}$. τ_{eq} is the transition point in time between the two zones and can also be described by the Damköhler number, which is when the ratio of the reaction rate over the advection rate is one (Boucher and Alves, 1959; Jennings, 1987; Steefel and Maher, 2009). The τ_{eq} for all ensembles is quantitatively defined here (Table 2) as the point at which the percent change in reaction rate from one cell to the next (where cell length represents residence time in the streamline transform) is <0.1%. τ_{eq} can also be thought of as the extent of the reaction front from the leak, which is an evolving result.

For the positively correlated and homogeneous conditions τ_{eq} equaled 481 days after 1000 days of simulation time and 482 days after 6000 days of simulation time. τ_{eq} for the negatively correlated case increased from 492 to 495 days over the duration of the simulation (Table 2). Thus, despite the influence of geochemical heterogeneity along each streamline, as represented by calcite surface area (Fig. 3), the weathering front is nearly static. This static weathering front is representative of conditions where the reduction of calcite volume and therefore reactive calcite surface area is not fast enough to deplete calcite at any point along the streamline. Calcite does not deplete in the first grid cells along the flow paths during the simulation, therefore we see little movement of the reaction front but would expect typical moving boundary behavior for this system at longer simulation times (Lichtner, 1988; Maher, 2010; White and Brantley, 2003). However, measurable calcite depletion and a corresponding reduction in calcite dissolution rates near the CO_2 source are observed as the simulations progress in time (Fig. 3). The decrease in calcite dissolution rates at short transport distances increases the geochemical disequilibrium at larger transport distances within the kinetic zone before τ_{eq} is achieved. This increase in disequilibrium at larger transport distances in turn increases the calcite dissolution rates at these larger distances before τ_{eq} is achieved (Fig. 3). Therefore, during the simulations presented here the total residence time and corresponding distance over which kinetic mineral reactions occur stays the same, as in a quasi-stationary state moving boundary condition (Lichtner, 1988).

3.2. Reactive plume evolution

The reactive plume in each realization is a collection of streamlines with unique residence times that make up the ensemble cumulative distribution of residence time at each plane and at the pumping well (Figs. 1 and 4). Given that physical heterogeneity determines the τ to L relationship for each streamline, Pb^{2+} concentration at any given transverse plane is then a product of a host of groundwater chemical conditions resulting from the cumulative distribution of residence time intersecting the plane. Consequently, the role that physical heterogeneities play in determining solute residence time and therefore the chemical condition at the plane may be especially important as aquifer conditions such as σ^2_{lnK}, covariance function, and aquifer stratification vary (Atchley et al., 2013a; Siirila et al., 2012). Here the residence time distribution at each plane and the well is identical for each heterogeneity scenario because the same 100 hydraulic conductivity fields were used for ensembles in each heterogeneity scenario.

By controlling for physical heterogeneity and inducing geochemical heterogeneity these simulations demonstrate the influence of heterogeneous geochemical conditions on reactive

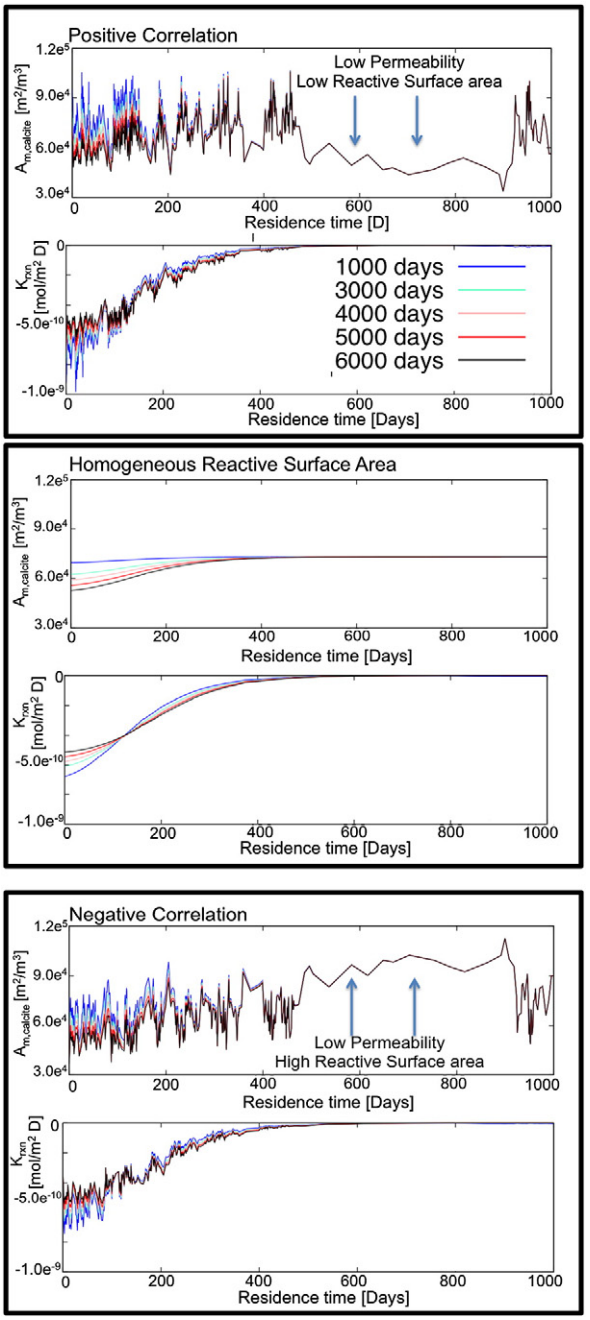

Fig. 3. Streamline profiles showing reactive surface areas and local-scale reaction rates for calcite. Positively correlated, homogeneous surface areas, and a negatively correlated profile are shown at 1, 3, 4, 5, and 6 thousand day simulation time increments. Because calcite dissolution equates to a negative reaction rate, areas of high reactive surface area will correspond to strongly negative reaction rates before equilibrium is met.

plume evolution in this system where the aquifer mineralogy itself is the source of contamination and not a point source as in much of the research on contaminant fate and transport (Cunningham and Fadel, 2007; Ginn et al., 1995; Maxwell et al., 2003; Siirila et al., 2012). Here we find that the Pb^{2+} flux through these planes and the pumping well varies with the three correlations of reactivity with heterogeneity (Fig. 5) and

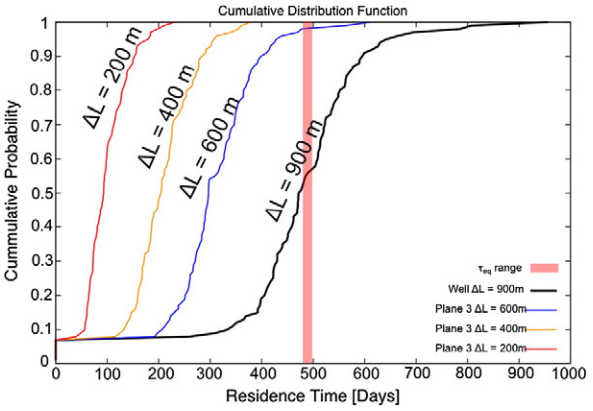

Fig. 4. Ensemble residence time cumulative distributions of all streamlines at each plane and pumping well, labeled by the advected distance from the CO_2 source. The residence time cumulative distributions are the same for each ensemble because each geochemical scheme was simulated on the same 100 physically heterogeneous realizations. The range of τ_{eq} listed in Table 2 for all 3 ensembles is plotted.

that the degree of Pb^{2+} flux difference between surface area distributions decreases with transport distance. Close to the source, where the reactive surface area influences geochemical reaction rates, dis-equilibrium between the fluids and aquifer mineralogical heterogeneity influences plume evolution. However, at points $> \tau_{eq}$ from the source where the fluids have re-equilibrated with the solids, plume evolution is a function of physical heterogeneity only. The residence time at the pumping well 900 m down gradient from the CO_2 source is essentially equal to the mean of the τ_{eq} for the three geochemical ensembles (Fig. 4). Therefore, steady-state Pb^{2+} mass flux at the pumping well in the three geochemical conditions varies by only 3.7×10^{-8} mol/day, but because not all the streamlines terminating at the pumping well have achieved equilibrium Pb^{2+} mass flux is still higher than the geochemical equilibrium (Fig. 5). Galena precipitation reduces the Pb^{2+} concentration along streamlines for all three geochemical conditions (Fig. 2) leading to a decrease in Pb^{2+} mass flux across the transverse planes further from the leak zone (Fig. 5).

In order to demonstrate how small scale geochemical heterogeneities influence large scale effective reaction rates, $K_{rxn,eff}$ was calculated for the three geochemical conditions using Eq. (5) and the median residence time for each plane shown in Fig. 6. At any point along the profile $K_{rxn,eff}$ represents the cumulative effect of the unique local K_{rxn} values in all streamlines at earlier residence times, which includes both precipitation and dissolution. Even though the domain average reactive surface areas are the same for each geochemical cases simulated (Table 1), the $K_{rxn,eff}$ varies between the three cases in the kinetic condition zone. Consistent with previous research (Dentz et al., 2011; Lichtner and Tartakovsky, 2003) the departure of reaction rates from zero, or geochemical equilibrium, decreases with residence time for all cases simulated (Fig. 6A and Table 2). For the scenario simulated here $K_{rxn,eff}$ is negative (mineral dissolution) at each plane despite galena precipitation through most of the domain. The decrease in $K_{rxn,eff}$ with residence time reflects the removal of Pb^{2+} from solution by this precipitation, thus $K_{rxn,eff}$ does not provide a complete picture of the geochemical reactions in the

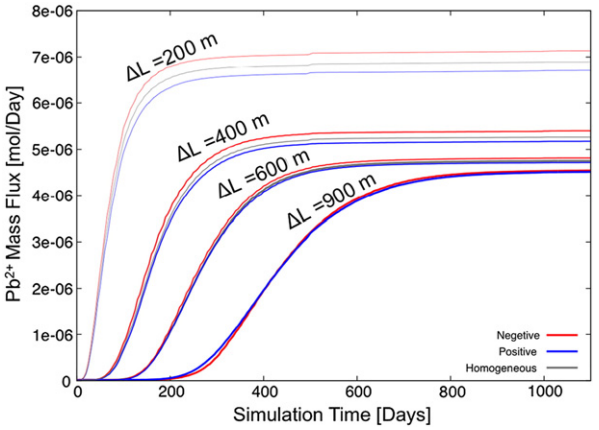

Fig. 5. Ensemble average breakthrough curves for all three geochemical ensembles are shown for each plane and the pumping well. Distance from the CO_2 source zone is listed corresponding to each plane or the pumping well.

subsurface. As $K_{rxn,eff}$ slows with residence time, the difference between $K_{rxn,eff}$ of each of the three scenarios also decreases from ~2% between the positively and negatively correlated surface areas and the homogeneous case to 0% between positively correlated surface area and homogeneous at ~400 days of residence time. The $K_{rxn,eff}$ difference between the negatively correlated surface area and the homogeneous case approaches 0% at ~600 days (Fig. 6B). This convergence of $K_{rxn,eff}$ results from the re-establishment of equilibrium by approximately 500 days of residence time for each geochemical scenario. Differences in $K_{rxn,eff}$ between the transverse planes within a given geochemical condition are ~5 times greater than the differences in $K_{rxn,eff}$ at the same plane in the three geochemical conditions.

Differences in $K_{rxn,eff}$ in these simulations where physical heterogeneity is the same in each geochemical scenario, but mineralogical heterogeneity varies help elucidate the role of geochemical and physical heterogeneities in complex reactive transport systems. In the positively correlated ensemble, reactions occur fast in areas where transport is also fast, which brings groundwater in preferential flow paths to near equilibrium conditions. Reactions are slow in streamlines with long residence times, but because residence times are also long, reactions have ample time to achieve equilibrium before reactive solute arrives at the transverse planes or pumping well. The net result is that groundwater in the positively correlated and the homogenous ensemble reaches equilibrium faster than the negatively correlated ensemble (Table 2). In the negatively correlated ensemble, reactions are fast in slow moving water and reach geochemical equilibrium relatively quickly even though solute has advected a short distance. However, groundwater in fast moving preferential flow paths reacts slowly and does not reach equilibrium prior to the transverse planes or pumping well. Moreover, because preferential flow paths have larger fluxes of water relative to slower moving flow paths (Atchley et al., 2013a; Moreno and Tsang, 1994) a larger portion of the water captured at the planes or pumping well is not at equilibrium even at larger travel distances for the negatively correlated ensemble. Therefore, the Pb^{2+} concentration and reaction rate at the pumping well are slightly higher for the negatively correlated case than the other two geochemical conditions simulated (Table 2).

Initial dissolution followed by precipitation of galena along the streamlines complicates the extrapolation of $K_{rxn,eff}$ to the subsurface processes. In these numerical simulations we know that galena dissolves in the first few cells and Pb^{2+} concentrations increase and that galena precipitates along the rest of the streamline reducing Pb^{2+} concentrations. However, the net increase of Pb^{2+} in solution results in $K_{rxn,eff}$ that indicates galena dissolution. Thus, a comparison between $K_{rxn,eff}$ for positively and negatively correlated surface areas in Table 2 suggests that galena dissolution rates are faster in the negatively correlated case relative to the positively correlated case. However, the faster $K_{rxn,eff}$ in the negatively correlated case is due to slower galena precipitation rates in the negatively correlated case, which results in slower Pb^{2+} concentration reductions along the streamline compared to the positively correlated case. As a result, it takes longer for the system to re-equilibrate when surface area is negatively correlated to hydraulic conductivity (Table 2). In cases where changes in solute concentrations are related to either mineral dissolution or precipitation, but not both, negatively correlating reactive surface area to permeability

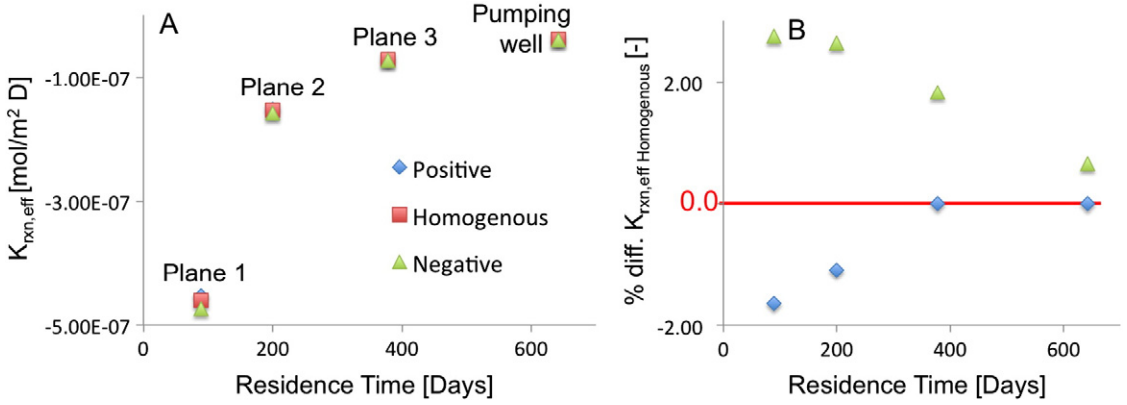

Fig. 6. Plot A shows the change in $K_{rxn,eff}$ for galena dissolution for each geochemical ensemble at the median residence time of each plane and the pumping well. $K_{rxn,eff}$ was calculated using Eq. (2). The plane and pumping well data points are labeled in plot A. Plot B shows the percent difference of each geochemical ensemble $K_{rxn,eff}$ of the homogeneous geochemical ensemble at the corresponding residence time for each plane and pumping well. Note that the $K_{rxn,eff}$ values converge as residence time increases.

will still result in a larger departure from equilibrium over the duration of the reaction path compared to positively correlated reactive surface areas in preferential flow paths (Fig. 7). Moreover, if the negative correlation of reactive surface area is strong enough, τ_{eq} and L_{eq} will also be extended in time. In this case, the $K_{rxn,eff}$ would be smaller in the negatively correlated case, which results in extending the reactive time scales and may in part be responsible for the reduction of $K_{rxn,eff}$ observed at field scales (Maher, 2011; Moore et al., 2012; Navarre-Sitchler and Brantley, 2007; Riebe et al., 2004).

Differences in heterogeneity distribution also give rise to differences in plume fingering (Fig. 8). In early to mid-plume development and residence times, fingering is more pronounced in the negatively correlated domains compared to the positively correlated domains. This observation agrees with previous findings (Cunningham and Fadel, 2007) and leads to a conceptual model of this system presented in Fig. 7. At long transport distances and late reaction times, the positively and negatively correlated Pb^{+2} concentration plumes are approximately the same (light blue segment of both the positively and negatively correlated plumes in Fig. 8). Three separate processes are working to cause the early to mid-transport differences and late transport similarities between the positively and negatively correlated plumes depicted in Fig. 8. First transport in the physically heterogeneous domains causes spreading in space and time, which in turn provides a physical structure for plume figuring to form. Second, the physical heterogeneity in the two heterogeneity distributions results in the fluid sampling a larger distribution of hydraulic conductivity (and therefore in the positively- and negatively-correlated plumes, reactive surface areas) over time. The difference between positively- and negatively-correlated plumes evolves as a function of length along the plume as the different geochemical cases sample an increasingly unique distribution of reactive surface areas (inset of Fig. 8). Third, the dissolving of calcite and precipitation of galena resulting in re-equilibration between the fluid and the minerals occurs along the flow path in each of the heterogeneity distribution cases, which slowly counters the heterogeneous developments of the first two processes. Thus, plume evolution far from the source ($\tau > \tau_{eq}$) is approximately the same regardless of heterogeneity distribution. The combined effect of these three processes (Fig. 7) results in noticeable differences in Pb^{2+} concentration in the early to mid-transport distances of the plumes (Fig. 8). Despite all three geochemical cases resulting in the same geochemical equilibrium, the specific τ_{eq} and plume evolution within the kinetic condition zone is unique for each case simulated. For example, negatively correlating reactive surface area to hydraulic conductivity extends the kinetic condition zone and the calcite buffering action. The slower buffering action in the negatively correlated case in turn slows galena precipitation and extends the plume fingering.

4. Summary and conclusions

Geochemical reactive plume development was investigated using a streamline approach to simulate coupled physical and geochemical heterogeneities. Three geochemical conditions were tested over an ensemble of 100 physically heterogeneous (hydraulic conductivity) realizations: a spatially homogeneous geochemical condition, and a reactive surface area positively and negatively correlated to hydraulic conductivity. Pb^{2+} concentrations, fluid residence times, and local reaction rates were examined to interpret the impact of local conditions on large-scale geochemical and hydrological processes. Results show that despite all three geochemical ensembles having the same domain average reactive surface area, plume evolution is unique for each ensemble; subsequently differences in Pb^{2+} concentrations at early to mid-transport times occur between the three ensembles. At late transport times, all three geochemical schemes Pb^{2+} concentrations become the same because the same geochemical equilibrium is achieved regardless of the spatial configuration of the geochemical conditions. However, because plume evolution toward geochemical equilibrium is unique for the three correlations of reactivity with heterogeneity, the transport time and length scales to achieve equilibrium, defined here as τ_{eq} and L_{eq} respectively, are also unique. Negatively correlating reactive surface areas to hydraulic conductivity had the longest τ_{eq} and L_{eq}, and positively correlating reactive surface areas to hydraulic conductivity and the shortest τ_{eq} and L_{eq}.

Two zones of large-scale reaction rates, $K_{rxn,eff}$, were delineated in the simulations (Figs. 2 and 7). The kinetic condition zone occurs prior to $\tau = \tau_{eq}$, where reaction kinetics contribute to the change in $K_{rxn,eff}$. The equilibrium condition zone occurs where $\tau > \tau_{eq}$ and residence time is the sole governor of $K_{rxn,eff}$. Within the kinetic condition zone, large-scale reaction rates varied between the three geochemical conditions because of

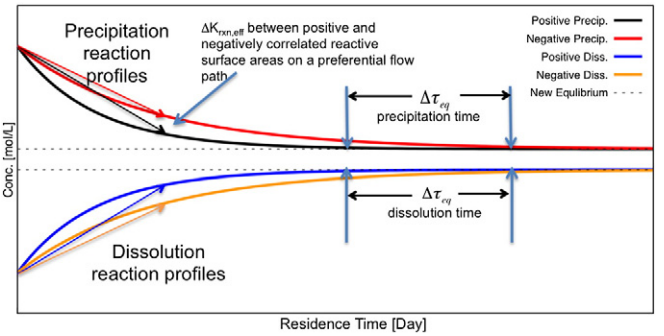

Fig. 7. Simplified reaction profiles for positively and negatively correlating reactive surface areas in a precipitation and dissolution reaction. $\Delta\tau_{eq}$ shows the changing time to equilibrium between the two geochemical cases. The slope of the arrows demonstrates the different $K_{rxn,eff}$ values for positively and negatively correlated profiles.

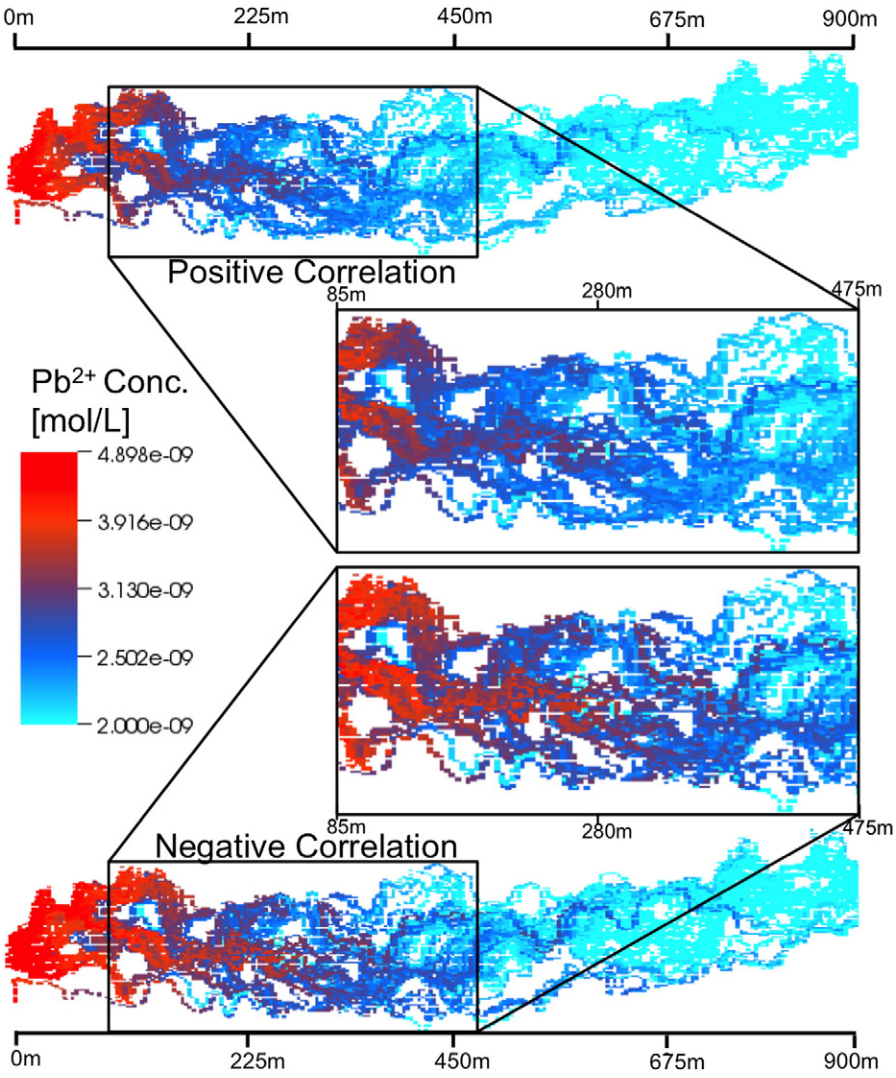

Fig. 8. Positively and negatively correlated plumes from the same physically heterogeneous domain are compared. The inset showcases the pronounced fingering and larger Pb^{2+} concentrations in the kinetic condition zone for the negatively correlated ensemble compared to the positively correlated case. Beyond the inset, Pb^{2+} concentrations are nearly the same between the positively and negatively correlated cases (depicted in light blue), because both cases achieve the new geochemical equilibrium.

the small-scale differences in reactive surface areas. This suggests that ignoring small-scale geochemical properties can be problematic for estimating larger-scale reactive plume conditions. However, once geochemical equilibrium is achieved, small-scale geochemical heterogeneities no longer actively affect plume characteristics. Conversely, spatial configurations of geochemical reactive surface areas can also influence τ_{eq} and L_{eq}, which extends the reactive portion of the plume. Therefore, defining the transport time scales where small-scale kinetic reactions can be neglected is difficult without first considering the physical and geochemical configurations.

In order to understand the overall plume development both physical and geochemical heterogeneities should be jointly considered. Here hydraulic conductivity heterogeneity was shown to provide a physical structure for plume fingering. The heterogeneous geochemical relationship to hydraulic conductivity can then decrease the observed fingering, as is the case for positively correlating reactive surface area to hydraulic conductivity, whereas negative correlation will result in pronounced plume fingering. These results are supported by studies of correlating heterogeneous biodegradation rates (Cunningham and Fadel, 2007; Maxwell et al., 2003; Scheibe et al., 2007). In the geochemical reactive transport system studied here, all reactions tend toward a new geochemical equilibrium. The result is that at some transport time or distance all configurations of geochemical reaction rates will arrive at the same reactive solute condition. However, the hydro-geochemical transport described above will contribute to the spatial evolution of a reactive plume, and therefore each physical and geochemical configuration will have unique τ_{eq} and L_{eq} scales at which reactions cease to occur.

Acknowledgments

This research has been supported by a grant from the US Environmental Protection Agency's Science to Achieve Results (STAR) program. Although the research described in the article has been funded wholly by the US Environmental Protection Agency's STAR program through Grant RD-83438701-0, it has not been subjected to any EPA review and therefore does not necessarily reflect the views of the Agency, and no official endorsement should be inferred. The authors would like to further thank the helpful and thorough reviews from John McCray, Magnus Skold, David Benson, and two anonymous reviewers.

References

Aagaard, P., Helgeson, H.C., 1982. Thermodynamic and kinetic constraints on reaction rates among minerals and aqueous solutions: I. Theoretical considerations. Am. J. Sci. 282, 237–285.

Allen-King, R.M., Halket, R.M., Gaylord, D.R., 1998. Characterizing the heterogeneity and correlation of perchloroethene sorption and hydraulic conductivity using a facies-based approach. Water Resour. Res. 34 (3), 385–396.

Apps, J.A., Zheng, L., Xu, T., Birkholzer, J.T., 2010. Evaluation of potential changes in groundwater quality in response to CO_2 leakage from deep geological storage. Transp. Porous Media 82, 215–246.

Atchley, A.L., Maxwell, R.M., Navarre-Sitchler, A.K., 2013a. Using streamlines to simulate stochastic reactive transport in heterogeneous aquifers: kinetic metal release and transport in CO_2 impacted drinking water aquifers. Adv. Water Resour. 52, 93–106. http://dx.doi.org/10.1016/j.advwatres.2012.09.005.

Atchley, A.L., Maxwell, R.M., Navarre-Sitchler, A.K., 2013b. Human health risk assessment of CO_2 leakage into overlying aquifers using a stochastic, geochemical reactive transport approach. Environ. Sci. Technol. 47 (11), 5954–5962. http://dx.doi.org/10.1021/es400316c.

Barber II, L.B., Thurman, E.M., Runnells, D.D., 1992. Geochemical heterogeneity and a sand and gravel aquifer: effect of sediment mineralogy and particle size on the sorption of chlorobenzenes. J. Contam. Hydrol. 9, 35–54.

Bearup, L.A., Navarre-Sitchler, A.K., Maxwell, R.M., McCray, J.E., 2012. Kinetic metal release from competing process in aquifers. Environ. Sci. Technol. 46, 6539–6547. http://dx.doi.org/10.1021/es203586y.

Boucher, d.F., Alves, G.E., 1959. Dimensionless numbers for fluid mechanics heat transfer, mass transfer and chemical reaction. Chem. Eng. Prog. 55, 55–64.

Carroll, S., Hao, Y., Aines, R., 2009. Geochemical detection of carbon dioxide in dilute aquifers. Geochem. Trans. 10, 4. http://dx.doi.org/10.1186/1467-4866-10-4.

Cirpka, O.A., Kitanidis, P.K., 2000. Characterization of mixing and dilution in heterogeneous aquifers by means of local temporal moments. Water Resour. Res. 36 (5), 1221–1236.

Crane, M.J., Blunt, M.J., 1999. Streamline-based simulations of solute transport. Water Resour. Res. 35, 3061–3078.

Cunningham, J.A., Fadel, Z.J., 2007. Contaminant degradation in physically and chemically heterogeneous aquifers. J. Contam. Hydrol. 94, 293–304.

Dagan, G., 1984. Solute transport in heterogeneous porous formations. J. Fluid Mech. 145, 151–177.

Dentz, M., Gouze, P., Carrera, J., 2011. Effective non-local reaction kinetics for transport in physically and chemically heterogeneous media. J. Contam. Hydrol. 120, 222–236. http://dx.doi.org/10.1016/j.jconhyd.2010.06.002.

Ginn, T.R., 2001. Stochastic-convective transport with nonlinear reactions and mixing: finite streamtube ensemble formulation for multicomponent reaction systems with intra-streamtube dispersion. J. Contam. Hydrol. 47, 1–28.

Ginn, T.R., Simmons, C.S., Wood, B.D., 1995. Stochastic-convective transport with nonlinear reaction: biodegradation with microbial growth. Water Resour. Res. 31 (11), 2689–2700.

Glassley, W.E., Simmins, A.M., Kercher, J.R., 2002. Mineralogical heterogeneity in fractured, porous media and its representation in reactive transport models. Appl. Geochem. 17, 699–708.

Holdren, G.R.J.R., Speyer, P.M., 1987. Reaction rate–surface area relationships during the early stages of weathering. II. Data on eight additional feldspars. Geochim. Cosmochim. Acta 51, 2311–2318.

Jennings, A.A., 1987. Critical chemical reactions rates for multicomponent groundwater contamination models. Water Resour. Res. 23 (9), 1775–1784.

Li, L., Peters, C.A., Celia, M.A., 2006. Upscaling geochemical reaction rates using pore-scale network modeling. Adv. Water Resour. 29, 1351–1370. http://dx.doi.org/10.1016/j.advwatres.2005.10.011.

Li, L., Peters, C.A., Celia, M.A., 2007. Effects of mineral spatial distribution on reaction rates in porous media. Water Resour. Res. 43. http://dx.doi.org/10.1029/2005WR004848.

Li, L., Steefel, C.I., Kowalsky, M.B., Englert, A., Hubbard, S.S., 2010. Effects of physical and geochemical heterogeneities in mineral transformation and biomass accumulation during biostimulation experiments at Rifle, Colorado. J. Contam. Hydrol. 112, 45–63.

Lichtner, P.C., 1988. The quasi-stationary state approximation to coupled mass transport and fluid–rock interaction in a porous medium. Geochim. Cosmochim. Acta 54, 143–165.

Lichtner, P.C., Tartakovsky, D.M., 2003. Stochastic analysis of effective rate constant for heterogeneous reactions. Stoch. Env. Res. Risk A. 17, 419–429.

Maher, K., 2010. The dependence of chemical weathering rates in fluid residence time. Earth Planet. Sci. Lett. 294, 101–110. http://dx.doi.org/10.1016/j.epsl.2010.03.010.

Maher, K., 2011. The role of fluid residence time and topographic scales in determining chemical fluxes landscapes. Earth Planet. Sci. Lett. 312, 48–58.

Maxwell, R.M., Welty, C., Tompson, A.F.B., 2003. Streamline-based simulation of virus transport resulting from long term artificial recharge in a heterogeneous aquifer. Adv. Water Resour. 26, 1075–1096. http://dx.doi.org/10.1016/S0309-1708(03)00074-5.

Maxwell, R.M., Welty, C., Harvey, R.W., 2007. Revisiting the Cape Cod bacteria injection experiment using a stochastic modeling approach. Environ. Sci. Technol. 41 (15), 5548–5558.

Meile, C., Tuncay, K., 2006. Scale dependence of reaction rates in porous media. Adv. Water Resour. 29, 62–71.

Mercado, A., 1967. The spreading pattern of injected water in a permeability stratified aquifer. Symposium of Haifa, Artificial Recharge and Management of Aquifers. IASH Publ. 72, 23–36.

Moore, J., Lichtner, P.C., White, A.F., Brantley, S.L., 2012. Using a reactive transport model to elucidate differences between laboratory and field dissolution rates in regolith. Geochim. Cosmochim. Acta 93, 235–261. http://dx.doi.org/10.1016/j.gca.2012.03.021.

Moreno, L., Tsang, C.-F., 1994. Flow channeling in strongly heterogeneous porous media: a numerical study. Water Resour. Res. 30 (5), 1421–1430. http://dx.doi.org/10.1029/93WR02978.

Navarre-Sitchler, A.K., Brantley, S., 2007. Basalt weathering across scales. Earth Planet. Sci. Lett. 261, 321–334. http://dx.doi.org/10.1016/j.epsl.2007.07.010.

Navarre-Sitchler, A., Steefel, C., Yang, L., Brantley, S., 2009. Evolution of porosity diffusivity during chemical weathering of a basalt clast. J. Geophys. Res. Earth Surf. 114. http://dx.doi.org/10.1029/2008JF001060 F02016.

Navarre-Sitchler, A.K., Steefel, C.I., Sak, P.B., Brantley, S.L., 2011. A predictive model for weathering rind formation on basalt. Geochim. Cosmochim. Acta 75, 7644–7667. http://dx.doi.org/10.1016/j.gca.2011.09.033.

Navarre-Sitchler, A.K., Maxwell, R.M., Siirila, E.R., Hammond, G.E., Lichtner, P.R., 2013. Elucidating geochemical response of shallow heterogeneous aquifers to CO_2 leakage using high-performance computing: implications for monitoring of CO_2 sequestration. Adv. Water Resour. 53, 45–55. http://dx.doi.org/10.1016/j.advwatres.2012.10.005.

Obi, E.-O.I., Blunt, M.J., 2006. Streamline-based simulation of carbon dioxide storage in a North Sea aquifer. Water Resour. Res. 42. http://dx.doi.org/10.1029/2004WR003347.

Riebe, C.S., Kirchner, J.W., Finkel, R.C., 2004. Erosional and climate effects on long-term chemical weathering rates in granitic landscapes spanning diverse climate regimes. Earth Planet. Sci. Lett. 224, 547–562. http://dx.doi.org/10.1016/j.epsl.2004.05.019.

Robin, M.J.L., Sudicy, R., Gillham, R., Kachanoski, R., 1991. Spatial variability of strontium distribution coefficients and their correlation with hydraulic conductivity in the Canadian Forces base Borden aquifer. Water Resour. Res. 27 (10), 2619–2632.

Rubin, Y., 1991. Transport in heterogeneous porous media: prediction and uncertainty. Water Resour. Res. 27 (7), 1723–1738.

Scheibe, T.D., Dong, H., Xie, Y.L., 2007. Correlation between bacterial attachment rate coefficients and hydraulic conductivity and its effect on field-scale bacterial transport. Adv. Water Resour. 30, 1571–1582. http://dx.doi.org/10.1016/j.advwatres.2006.05.021.

Seeboonruang, U., Ginn, T.R., 2006. Upscaling heterogeneity in aquifer reactivity via exposure-time concept: forward model. J. Contam. Hydrol. 84, 127–154.

Siirila, E.R., Maxwell, R.M., 2012. Evaluating effective reaction rates of kinetically driven solutes in large-scale, statistically anisotropic media: human health risk implications. Water Resour. Res. 48, W04527. http://dx.doi.org/10.1029/2011WR011516.

Siirila, E.R., Navarre-Sixtchler, A.K., Maxwell, R.M., McCray, J.E., 2012. A quantitative methodology to assess the risks to human health from CO_2 leakage into groundwater. Adv. Water Resour. 36 (2), 146–164. http://dx.doi.org/10.1016/j.advwatres.2010.11.005.

Steefel, C.I., 2001. Software for Modeling Multicomponent, Multidimensional Reactive Transport. Lawrence Livermore National Laboratory, Livermore, Ca (UCRL-MA-143182).

Steefel, C.I., Lasaga, A.C., 1994. A coupled model for transport of multiple chemical-species and kinetic precipitation dissolution reactions with application to reactive flow in single-phase hydrothermal systems. Am. J. Sci. 294 (5), 529–592.

Steefel, C.I., Maher, K., 2009. Fluid–rock interaction: a reactive transport approach. Reviews in Mineralogy & Geochemistry. Mineralogical Society of America, pp. 485–532.

Steefel, C.I., Yabusaki, S.B., 1996. OS3D/GIMRT, Software for Multicomponent–Multidimensional Reactive Transport: User's Manual and Programmer's Guide. Pacific Northwest National Laboratory, Richland, Washington (PNL-11166).

Steefel, C.I., DePaolo, D.J., Lichtner, P.C., 2005. Reactive transport modeling: an essential tool and new research approach for the Earth sciences. Earth Planet. Sci. Lett. 240, 539–558.

Sudicky, E.A., 1986. A natural gradient experiment on solute transport in a sand aquifer: spatial variability of hydraulic conductivity and its role in dispersion process. Water Resour. Res. 22 (13), 2069–2082.

Thiele, M.R., Batycky, R.P., Blunt, M.J., Orr Jr., F.M., 1996. Simulating flow in heterogeneous systems using streamtubes and streamlines. SPE Reserv. Eng. 11 (1), 5–12.

Tompson, A.F.B., Schafer, A.L., Smith, R.W., 1996. Impacts of physical and chemical heterogeneity on cocontaminant transport in a sandy porous medium. Water Resour. Res. 32 (4), 801–818.

Valocchi, A.J., 1989. Spatial moment analysis of the transport of kinetically and sorbing solutes through stratified aquifers. Water Resour. Res. 25 (2), 273–279.

van der Zee, S.E.A.T.M., van Remsdijk, W.H., 1991. Transport of reactive solute in spatially variable soil systems. Water Resour. Res. 23 (11), 2059–2069.

Viswanathan, H.S., Valocchi, A.J., 2004. Comparison of streamtube and three-dimensional models of reactive transport in heterogeneous media. J. Hydraul. Res. 42, 141–145.

Wang, S., Jaffe, P.R., 2004. Dissolution of a mineral phase in potable aquifers due to CO_2 releases from deep formations; effect of dissolution kinetics. Energ. Convers. Manage. 54, 2833–2848.

White, A.F., Brantley, S.L., 2003. The effect of time on the weathering of silicate minerals: why do weathering rates differ in the laboratory and field? Chem. Geol. 202, 479–506.

Wilkin, R.T., Digiulio, D.C., 2010. Geochemical impacts to groundwater from geologic carbon sequestration: controls on pH and inorganic carbon concentrations from reaction path and kinetic modeling. Environ. Sci. Technol. 44 (12), 4821–4827.

Yeh, T.-C.J., 1992. Stochastic modeling of groundwater flow and solute transport in aquifers. Hydrol. Process. 6, 369–395.

Zheng, L., Apps, J.A., Zhang, Y., Xu, T., Birkholzer, J.T., 2009. On mobilization of lead and arsenic in groundwater in response to CO_2 leakage from deep geological storage. Chem. Geol. 268, 281–297. http://dx.doi.org/10.1016/j.chemgeo.2009.09.007.